

## Fermi level pinning for zinc-blende semiconductors explained with interface bonds

Raymond T. Tung<sup>1,\*</sup> and Leeor Kronik<sup>2,†</sup>

<sup>1</sup>*Department of Physics, Brooklyn College, CUNY, Brooklyn, New York 11210, USA*  
 and *Physics Ph.D. Program, Graduate Center, CUNY, New York, New York 10016, USA*

<sup>2</sup>*Department of Materials and Interfaces, Weizmann Institute of Science, Rehovoth 76100, Israel*



(Received 13 September 2020; revised 22 November 2020; accepted 19 January 2021; published 1 February 2021)

Schottky barrier heights (SBHs) measured at polycrystalline metal-semiconductor (MS) interfaces have displayed an insensitivity to the work function (WF) of the metal, known as the “Fermi level pinning” (FLP) phenomenon. The obstacle presented by FLP in thwarting technological efforts to tune the SBH has been difficult to overcome because of a lack of understanding of the origin of the FLP effect. Presently, SBH explanation still largely relies on empirical models, and FLP remains a mystery. Here, the phenomenon of FLP for zinc-blende/diamond (ZBD) semiconductors is explicitly demonstrated to originate from interface metal-cation bonds, which are metallic in nature. Based on the analysis of two representative and electrically distinct types of interface, it is shown that screening by metallic bonds weakens the dependence of SBH on the metal and results in a SBH close to that found between the semiconductor and its own cation in elemental metal form. The latter SBH is shown to agree well with experimentally measured SBH from polycrystalline interface, i.e., the apparent pinning levels. A fundamental, self-consistent explanation of the FLP phenomenon thus emerges, and with it, strategies to avoid FLP for technological applications may also be suggested.

DOI: [10.1103/PhysRevB.103.085301](https://doi.org/10.1103/PhysRevB.103.085301)

The observation of the Fermi level pinning (FLP) phenomenon, namely an insensitivity of the Schottky barrier height (SBH) to the work function (WF) at polycrystalline metal-semiconductor (MS) interfaces, has dominated the early experimental scenes of SBH research and has motivated the proposal of various empirical models to specifically account for this effect [1–4]. The most popular of these models assumed that a charge neutrality level (CNL) of the semiconductor marks the observed pinning level [3,5]. However, there is no known underlying justification for the CNL concept. Following the discovery of a sharp dependence of the SBH on the atomic structure at the epitaxial MS interface [6–9] and detailed analyses of polycrystalline interfaces [7,10–12], it is now clear that the SBHs at nonepitaxial MS interfaces are spatially inhomogeneous. Therefore, experimental observation of FLP only indicates that the average of the SBH distribution at polycrystalline interfaces does not depend strongly on the metal. Because, in general, the magnitude of the SBH is a direct result of the distribution of charge at an MS interface [13,14], which in turn is governed by quantum mechanics, all SBH behavior should have an explanation based on general chemical principles of bond formation. Reliance on empirical theories should not be necessary. Indeed, we showed very recently that SBHs at epitaxial MS interfaces could be explained quantitatively based on the polarization of interface bonds estimated by simple chemical arguments, once the surface dipole terms from the metal WF and the semiconductor ionization potential (IP) were removed [15]. Motivated by these

recent discoveries, here, we show that the entire FLP phenomenon, including the weakened SBH dependence on the metal and the apparent pinning level for each semiconductor, also has an explanation from chemical bonds.

The *p*-type SBH,  $\phi_{B,p}$ , for a noninteracting MS interface is given by Schottky-Mott theory (SMT) to be the difference between the semiconductor IP ( $I_{SC}$ ) and the metal WF ( $\phi_M$ ). Effects due to chemical equilibration lead to a correction to the SMT, in the form of a charge-distribution-dependent electrostatic interface dipole,  $\Delta_{ISR}$ , that arises at the interface-specific region (ISR):

$$\phi_{B,p} = I_{SC} - \phi_M + \Delta_{ISR}. \quad (1)$$

Note that defining a dipole at a MS interface is somewhat arbitrary because, as pointed out previously [14,16], both WF and IP contain surface dipole contributions unconnected with properties of the MS interface. As a result,  $\Delta_{ISR}$  also contains these surface dipole contributions.

Recently, *p*-type SBHs for many epitaxial interfaces between metals (alloys) and semiconductors with zinc-blende/diamond (ZBD) structure were calculated [15]. Among those, 12 metal-ZBD systems calculated in the (100) orientation with both metal-cation and metal-anion geometries are analyzed in this paper. Additional structures, including supercells, surfaces, and other specific structures, are studied here in support of the analysis. All results are from density functional theory calculations, performed with a plane-wave basis and a projector augmented wave treatment of core electrons as implemented in the Vienna *ab initio* Simulation Package (VASP) [17–20]. Details of computations were previously described [15,21,22] and may also be found in the Supplemental Material (SM) [23].

\*rtung@brooklyn.cuny.edu

†leeor.kronik@weizmann.ac.il

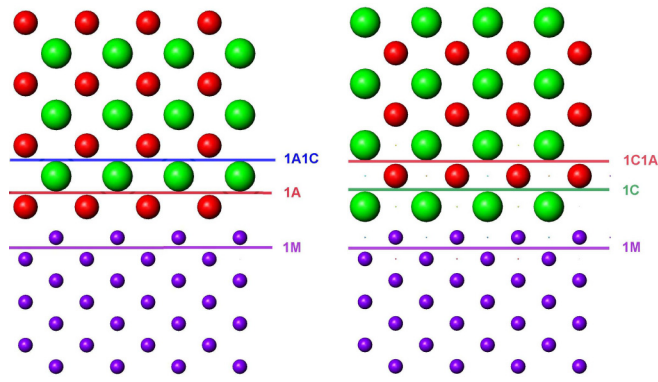


FIG. 1. Models of the stacking sequence at epitaxial metal-zinc-blende (100) interface: small sphere = metal, medium sphere = anion, large sphere = cation. Neither the drawing on left for metal-anion (100) interface, nor that on right for metal-cation (100) interface necessarily corresponds to the actual atomic structure used in the calculations. Lines mark locations where the metal-semiconductor structure may be cut for determination of the range of interface dipole.

A polycrystalline MS interface that displays FLP has a single crystal semiconductor on one side and a metallic layer with spatially varying crystal orientation and structure on the other. On the metal side of the interface, the atomic structure varies laterally over a considerable depth. The width of the ISR, atoms within which are involved in the formation of the interface dipole, is not known *a priori*. If many layers of atoms were involved, the SBH problem would be essentially beyond the realm of simple chemical theories. Recent successes in quantitative modeling of the SBH at epitaxial MS interfaces from bond polarization, however, suggest that the formation of interface dipole likely involves only the first semiconductor layer and the first metal layer at the interface [15]. Under such a circumstance, a crucial factor for SBH formation is whether that layer of metal is bonded to the cation or the anion of the semiconductor. The metal-cation (100) and metal-anion (100) interfaces thus represent two distinct structures, the significantly different SBHs of which are likely on opposite ends of the range over which the SBH may vary at a polycrystalline interface. Therefore, they form a reasonable knowledge base from which the likely mechanism behind the FLP phenomenon may be deciphered. To do so, we need to first gain a firm understanding of the spatial extent (length) of dipoles at MS (100) interfaces.

Schematic diagrams of the two interfaces presently investigated are shown in Fig. 1. To determine the length of charge transfer at each interface, we draw two trial demarcation lines that define a neutral ISR that is as small as possible. When the charge transfer is indeed contained within, the chosen boundaries for the ISR would be, by definition, neutral or “bulklike.” Conversely, locations that are found not to be bulklike are still part of the ISR. To put this idea into practice, we recall that a bulk metal crystal can be cut in half, and the two exposed surfaces would be neutral and identical in every aspect. The potentials of the two half crystals can then be added together, or “stitched,” leaving no overall (long-range) potential shift across the location of the cut.

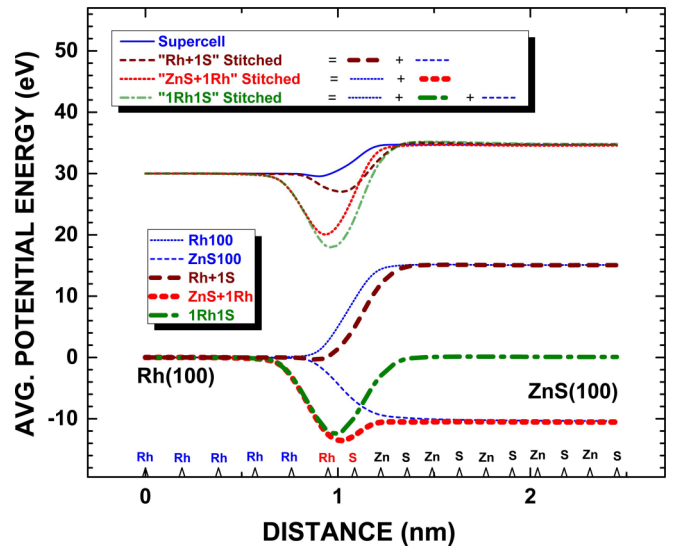


FIG. 2. Macroscopically averaged potential energy profiles of various structures associated with the Rh/ZnS(100) interface with Rh-S bonds. All curves are averaged over the repeating distances in both the ZnS(100) and the strained Rh(100) crystals. The profile marked “supercell” is obtained from calculation of the entire structure. Locations of the atomic planes are marked on the bottom. Other calculations are based on the same (super) unit cell but with specified layers of atoms removed. “Rh + 1S” is calculated with all semiconductor planes, marked in black on bottom, removed. “ZnS + 1Rh” is calculated with all Rh planes marked in blue removed. “1Rh1S” is obtained with all planes removed, except the two interface planes marked in red. Lines marked “stitched” are the result of stitching two or more lines together, as illustrated symbolically in the legend box. Upper curves have been shifted vertically for clarity. See Fig. SM-1 in the Supplemental Material [23] for a magnified view of the difference curve between stitched and supercell calculations.

A bulk ZB semiconductor crystal behaves the same way if the cut is along a nonpolar (110) plane. Cutting along the polar (100) plane, however, exposes the inequivalent cation-terminated and anion-terminated surfaces on the two sides, which can no longer be stitched together without an overall potential shift. Nevertheless, a cation-terminated (100) surface can always be stitched with another cation-terminated (100) surface, and anion-terminated with anion-terminated, without a long-range potential shift. With this in mind, we can cut the structure shown in Fig. 1 at any chosen location into two halves. If the potential distributions for the two halves, calculated separately, can be added to approximately reproduce an overall potential shift of the original (uncut) supercell, then the location of the cut is considered neutral. If the stitched potential shift deviates considerably from that of the supercell, then the location of the cut is still part of the ISR.

We demonstrate this approach with the example of Fig. 2, which shows macroscopically averaged potential energy distributions arising from various components of the Rh/ZnS(100) interface with Rh-S bonds. All curves are first plane averaged and then averaged in the longitudinal direction, over the repeating distances in both the ZnS(100) and the strained Rh(100) crystals [24]. To find out whether the



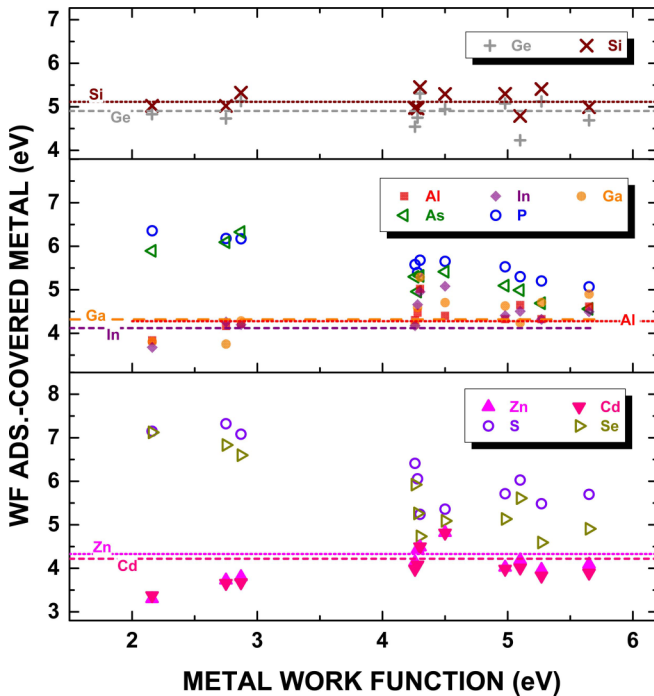


FIG. 4. Work function (WF) of various metal (100) surfaces covered with one monolayer of adsorbate, plotted against the WF of the bare metal. (a) Group IV adsorbates, (b) group III and V adsorbates, and (c) group II and VI adsorbates. Horizontal lines mark the WFs of the metallic surface of elemental group II, III, and IV elements.

The above analysis suggests that the properties of metal surfaces with a layer of adsorbates may be crucial for the explanation of SBH formation. To understand the distinctly different behavior of metal-cation and metal-anion interfaces, metal surfaces covered with cation and anion adsorbates have been systematically studied. For WF calculations, adsorbate atoms were placed at the next lattice site of the metal (100) surface, and no relaxations were allowed. These results are shown in Fig. 4, as a function of the WF of the underlying metal. Note that without lattice relaxation and site optimization, Fig. 4 does not necessarily reproduce the WF observed in surface experiments [26–28]. Nonetheless, the information therein is vital for SBH interpretation. Opposite trends are observed in the figure: the WF of the anion-covered surface decreases with the WF of the underlying metal, whereas the opposite is generally true for the cation-covered surface. These opposing trends cannot both be explained with electronegativity differences and point to a fundamental difference between the metal-cation and the metal-anion bonds. Because cations are metals on their own, it is known that the WF of the underlying metal changes toward that of the adsorbate with increasing surface coverage. Experimentally, these WF changes take place rapidly and typically saturate well before one full layer [27,28]. Previous studies thus suggest that the WFs of cation-covered surfaces correspond approximately to that of the cations, which are marked by horizontal lines in Fig. 4, with some residual effect due to the substrate metal. Group IV adsorbates, similar to metallic cations, are found to significantly reduce the dependence of the WF on metal, likely because the free surfaces of Si and Ge are metallic [29]. An ex-

amination shows that the  $\sim 3.5$  eV range in the WFs of the underlying metal is reduced to  $\sim 1$  eV with group IV adsorbates,  $\sim 1.5$  eV with group III adsorbates, and  $\sim 2$  eV with group II adsorbates. Delocalized electrons throughout the metal and metallic adsorbate lead to equalization of the Fermi level and significantly screen out properties of the substrate metal. Interface metallicity agrees well with the recent observation that successful modeling of the SBHs at metal-cation (100) interfaces requires treating the interface dipole as arising between the semiconductor and the cation-adsorbed metal [15].

Further insight into the difference between metal-cation and metal-anion interfaces is obtained by recalling that, although the atomic structure and ensuing electron density is well defined for all interfaces studied, there is inherently no unique location where “the metal ends and the semiconductor begins.” This is because tunneling of metallic wave functions into the semiconductor necessarily obscures the spatial boundary for states at the Fermi level, the existence of which defines a metal. Such evanescent waves are also behind the well-known phenomenon of metal-induced gap states [30]. A comparison of the extent of metallic state decay into the semiconductor gap is given in Fig. 5 for three metals with widely different WFs and two representative semiconductors, AlP and ZnS. In all cases, a clear separation between charge density tails at the metal-cation interfaces and the metal-anion interfaces is observed. For each MS system, the exponential decay (i.e., slope of the semilogarithmic curves in the figure) is comparable for the metal-cation and the metal-anion interfaces. However, there is an approximately rigid shift of the metal-cation tails, by  $>0.2$  nm, toward the semiconductor, which is larger than the distance between the cation and anion (100) planes in these semiconductors ( $\sim 0.15$  nm). The results of Fig. 5 therefore strongly suggest that “metallicity” extends deeper into the semiconductor at the metal-cation interface than at the metal-anion interface. This corroborates the attribution of the different systematic trends in SBH for these two types of interface to spatial difference in interface metallicity.

The markedly different behavior at metal-cation and metal-anion interfaces, which offers clues to the origin of FLP, may be summarized as follows: (1) The dipole at a metal-anion interface is essentially confined to the interface metal and anion planes, and it may be quantitatively reproduced through chemical bond modeling. However, the trend of metal-anion SBH with the metal WF is opposite to that observed in polycrystalline experiments. (2) At metal-cation interfaces, dipole formation involves at least the next anion plane. Cations at the interface behave in a metallike fashion and significantly screen the metal WF. The (weakened) dependence of the metal-cation SBH on the metal WF is of the same sign as that observed experimentally for FLP.

Exploring the above leads further, one may ask: What would the SBH of a semiconductor, averaged over all metals (i.e., its pinning level), be if the interface structure were indeed dominated by metal-cation bonds? From (2) above, the answer is that it would be the SBH between the semiconductor and its own cation (in elemental metal form). This is a quantity that can be, and is presently, calculated for each semiconductor. Except for the Al/AIAs system, there is no lattice-matching condition between a semiconductor and its cation. These interfaces are still calculated epitaxially, with the metal in a

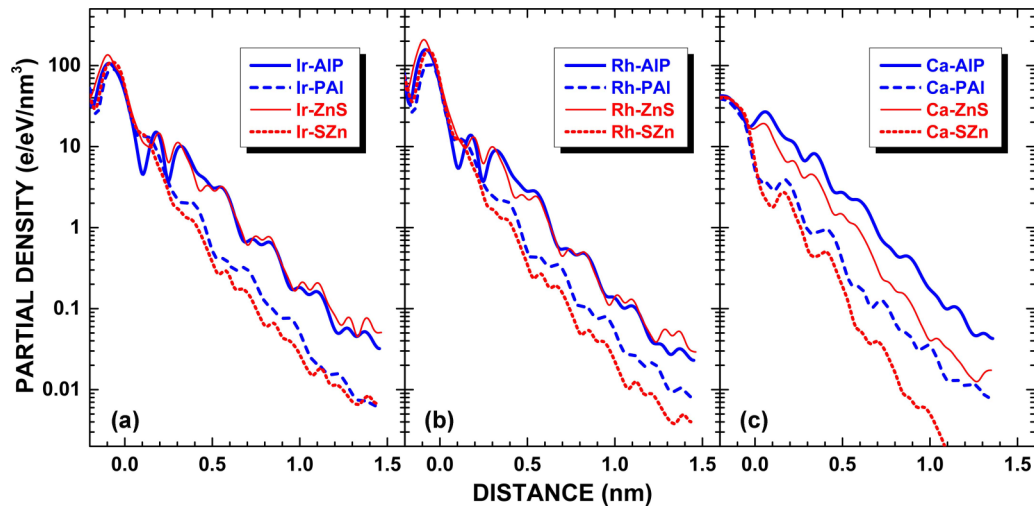


FIG. 5. Plane-averaged charge density of interface states with energy in the band gap of the semiconductor at the epitaxial (100) interfaces of AIP and ZnS with (a) Ir, (b) Rh, and (c) Ca for metal-cation (solid lines) and metal-anion (dashed lines) interfaces. Zeros on the horizontal axis mark the locations midway between the last metal plane on the left and the first semiconductor plane on the right. The density tail at metal-cation interfaces extends further into the semiconductor than that at metal-anion interfaces.

strained face-centered cubic structure (see methods in the SM for details [23]). As mentioned above, for elemental Si and Ge, there is no bulk metallic form *per se*, but the free surfaces are metallic and have WFs, toward which the underlying metals with adsorbed Si or Ge converge (see Fig. 4). Therefore, the difference between the Fermi level and the valence band maximum (VBM) at the surface of Si and Ge may be regarded as the *p*-type SBH between the semiconductor and the metallic form of itself. It should be noted that, similar to Si and Ge, the free surfaces of cation-terminated ZB (100) are also metallic and have Fermi level positions that are in general agreement with those calculated from supercells of ZB and cation. These calculated cation SBHs are compared with experimentally observed pinning levels in Fig. 6.

The excellent agreement shown in Fig. 6 strongly suggests that the metal-cation structure dominates polycrystalline ZBD interfaces and is responsible for the FLP. However, one still needs to justify the prevalence of this structure at polycrystalline interfaces. Present calculations show that, for most systems, the metal-anion (100) interfaces are favored energetically over the metal-cation (100) interfaces. However, this does not imply that common polycrystalline interfaces would be dominated by metal-anion bonds because the formation process of the physical interface follows kinetic paths that depend on many other factors. Decomposition of the semiconductor surface from metal deposition is quite common, as are compound formation and surface segregation. It is well documented that, in controlled clean experiments, both cations and anions are released upon metal deposition, and anions have a persistent tendency to segregate to the external metal surface [48–51], thereby leaving the interface cation rich. Coupled with the fact that the heats of formation for metal-anion compounds are generally larger than metal-cation compounds [52], these results make it plausible that randomly formed MS interfaces of any orientation contain a high percentage of metal-cation structure, resulting in the FLP phenomenon. In short, the metallicity of the metal-cation bonds screens and weakens the dependence of the SBH on metal WF, which

is the very definition of FLP, and leads to an average SBH close to that between the semiconductor and its own cation. With the reason for the FLP identified, obvious strategies to avoid FLP and tune the SBH also emerge. The use of “soft” metallization technologies [53–55], anion-containing metallic compounds [8], or chemically stabilized semiconductor surfaces [56,57] likely preserve the integrity of the surface during metallization, thereby reducing the tendency for metal-cation bonds and FLP.

In conclusion, analysis of many epitaxial interfaces between elemental metals and ZBD semiconductors reveals that the markedly different SBH behavior displayed at the

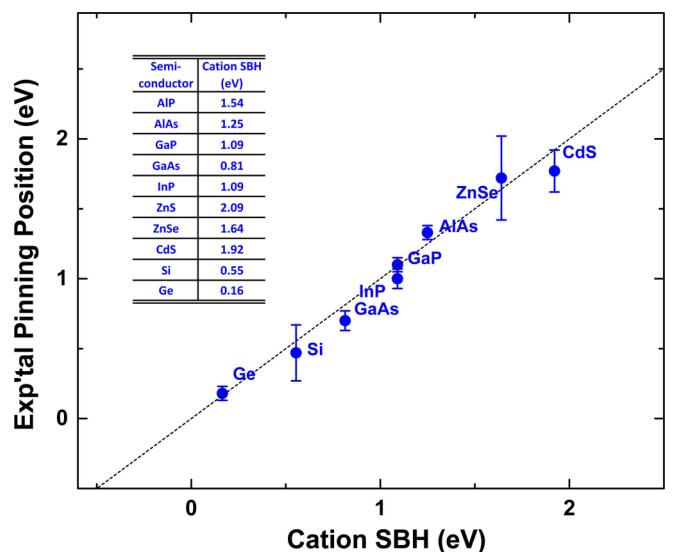


FIG. 6. Experimentally measured average *p*-type Schottky barrier height (SBH), shown against the *p*-type SBH calculated for each semiconductor with its own cation. See text for Si and Ge. Experimental results are adopted from the literature: InP [31,32], GaAs [33–35], ZnSe [36–38], Si [39–41], Ge [42,43], GaP [44], AlAs [45], and CdS [46,47].

metal-anion and metal-cation interfaces can be attributed to the metallic nature of interface bonds at the latter. The presence of these metallic interface bonds fully accounts for both hallmarks of FLP: the weakened dependence of the SBH on the metal and the apparent pinning level. Taken together with prior evidence for the prevalence of metal-cation bonds at the

MS interface, these calculations and analyses shed considerable light on the mystery surrounding the FLP phenomenon.

We thank A. Savin for assistance with the interpretation of interface metallicity from electron localization function analysis.

- 
- [1] J. Bardeen, *Phys. Rev.* **71**, 717 (1947).
- [2] W. E. Spicer, I. Lindau, P. Skeath, and C. Y. Su, *J. Vac. Sci. Technol.* **17**, 1019 (1980).
- [3] J. Tersoff, *Phys. Rev. Lett.* **52**, 465 (1984).
- [4] J. Tersoff and W. A. Harrison, *Phys. Rev. Lett.* **58**, 2367 (1987).
- [5] J. Robertson, *J. Vac. Sci. Technol. A* **31**, 050821 (2013).
- [6] R. T. Tung, *Phys. Rev. Lett.* **52**, 461 (1984).
- [7] R. T. Tung, A. F. J. Levi, J. P. Sullivan, and F. Schrey, *Phys. Rev. Lett.* **66**, 72 (1991).
- [8] C. J. Palmstrom, T. L. Cheeks, H. L. Gilchrist, J. G. Zhu, C. B. Carter, B. J. Wilkens, and R. Martin, *J. Vac. Sci. Technol. A* **10**, 1946 (1992).
- [9] H. Fujitani and S. Asano, *Phys. Rev. B* **42**, 1696 (1990).
- [10] R. T. Tung, *Phys. Rev. B* **45**, 13509 (1992).
- [11] J. P. Sullivan, R. T. Tung, M. R. Pinto, and W. R. Graham, *J. Appl. Phys.* **70**, 7403 (1991).
- [12] A. Olbrich, J. Vancea, F. Kreupl, and H. Hoffmann, *Appl. Phys. Lett.* **70**, 2559 (1997).
- [13] L. J. Brillson, *Surf. Sci. Rep.* **2**, 123 (1982).
- [14] R. T. Tung, *Mater. Sci. Eng. Rep.* **35**, 1 (2001).
- [15] R. T. Tung and L. Kronik, *Phys. Rev. B* **103**, 035304 (2021).
- [16] C. Mailhot and C. B. Duke, *Phys. Rev. B* **33**, 1118 (1986).
- [17] G. Kresse and J. Hafner, *Phys. Rev. B* **49**, 14251 (1994).
- [18] G. Kresse and D. Joubert, *Phys. Rev. B* **59**, 1758 (1999).
- [19] J. P. Perdew, K. Burke, and M. Ernzerhof, *Phys. Rev. Lett.* **77**, 3865 (1996).
- [20] J. Heyd, G. E. Scuseria, and M. Ernzerhof, *J. Chem. Phys.* **118**, 8207 (2003).
- [21] R. T. Tung and L. Kronik, *Phys. Rev. B* **94**, 075310 (2016).
- [22] R. T. Tung and L. Kronik, *Phys. Rev. B* **99**, 115302 (2019).
- [23] See Supplemental Material at <http://link.aps.org/supplemental/10.1103/PhysRevB.103.085301> for details of DFT calculations, analysis of macroscopically averaged potential energy profiles, plane-averaged charge density distributions, and calculated *p*-type SBHs of relaxed epitaxial metal-cation (100) interfaces.
- [24] M. Peressi, N. Binggeli, and A. Baldereschi, *J. Phys. D* **31**, 1273 (1998).
- [25] R. T. Tung, *Appl. Phys. Rev.* **1**, 011304 (2014).
- [26] J. B. Taylor and I. Langmuir, *Phys. Rev.* **44**, 423 (1933).
- [27] E. P. Gyftopoulos and J. D. Levine, *J. Appl. Phys.* **33**, 67 (1962).
- [28] H. Gerischer, D. M. Kolb, and M. Przasnyski, *Surf. Sci.* **43**, 662 (1974).
- [29] G. P. Srivastava, *Rep. Prog. Phys.* **60**, 561 (1997).
- [30] S. G. Louie, J. R. Chelikowsky, and M. L. Cohen, *Phys. Rev. B* **15**, 2154 (1977).
- [31] E. Hokelek and G. Y. Robinson, *J. Appl. Phys.* **54**, 5199 (1983).
- [32] N. Newman, M. Van Schilfgaarde, and W. E. Spicer, *Phys. Rev. B* **35**, 6298 (1987).
- [33] J. R. Waldrop, *Appl. Phys. Lett.* **44**, 1002 (1984).
- [34] N. Newman, M. van Schilfgaarde, T. Kendelwicz, M. D. Williams, and W. E. Spicer, *Phys. Rev. B* **33**, 1146 (1986).
- [35] A. B. McLean and R. H. Williams, *J. Phys. C* **21**, 783 (1988).
- [36] I. M. Dharmadasa, C. J. Blomfield, R. Coratger, E. Ajustron, J. Beauvillain, J. Simpson, K. A. Prior, and B. C. Cavenett, *Mater. Sci. Technol.* **12**, 86 (1996).
- [37] D. D. Nedeoglo, D. H. Lam, and A. V. Simashkevich, *Phys. Status Solidi A* **44**, 83 (1977).
- [38] M. S. Tyagi and S. N. Arora, *Phys. Status Solidi A* **32**, 165 (1975).
- [39] W. Mönch, *Surf. Sci.* **21**, 443 (1970).
- [40] P. E. Schmid, *Helv. Phys. Acta* **58**, 371 (1985).
- [41] R. T. Tung, *J. Vac. Sci. Technol. B* **11**, 1546 (1993).
- [42] A. Dimoulas, P. Tsipas, A. Sotiropoulos, and E. K. Evangelou, *Appl. Phys. Lett.* **89**, 252110 (2006).
- [43] T. Nishimura, K. Kita, and A. Toriumi, *Appl. Phys. Lett.* **91**, 123123 (2007).
- [44] M. von der Emde, D. R. T. Zahn, Ch. Schultz, D. A. Evans, K. Horn, *Appl. Surf. Sci.* **70–71**, 507 (1993).
- [45] W. I. Wang, *J. Vac. Sci. Technol. B* **1**, 574 (1983).
- [46] N. M. Forsyth, I. M. Dharmadasa, Z. Sobiesierski, and R. H. Williams, *Semicond. Sci. Technol.* **4**, 57 (1989).
- [47] W. G. Spitzer and C. A. Mead, *J. Appl. Phys.* **34**, 3061 (1963).
- [48] I. M. Vitomirov, C. M. Aldao, Z. Lin, Y. Gao, B. M. Trafas, and J. H. Weaver, *Phys. Rev. B* **38**, 10776 (1988).
- [49] F. Xu, J. J. Joyce, M. W. Ruckman, H.-W. Chen, F. Boscherini, D. M. Hill, S. A. Chambers, and J. H. Weaver, *Phys. Rev. B* **35**, 2375 (1987).
- [50] C. Bourgonon, S. Tatarenko, J. Cibert, L. Carbonell, V. H. Etgens, M. Eddrief, B. Gilles, A. Marty, and Y. Samson, *Appl. Phys. Lett.* **76**, 1455 (2000).
- [51] C. Heske, U. Winkler, R. Fink, E. Umbach, Ch. Jung, and P. R. Bressler, *Phys. Rev. B* **56**, 2085 (1997).
- [52] Z. Lin, F. Xu, and J. H. Weaver, *Phys. Rev. B* **36**, 5777 (1987).
- [53] H. Hasegawa, T. Sato, and T. Hashizume, *J. Vac. Sci. Technol. B* **15**, 1227 (1997).
- [54] H. Hasegawa, T. Sato, and S. Kasai, *Appl. Surf. Sci.* **166**, 92 (2000).
- [55] H. Haick, M. Ambrico, J. Ghabboun, T. Ligonzo, and D. Cahen, *Phys. Chem. Chem. Phys.* **6**, 4538 (2004).
- [56] E. Kaxiras, *Phys. Rev. B* **43**, 6824 (1991).
- [57] Y. Li, W. Long, and R. T. Tung, *Solid State Commun.* **151**, 1641 (2011).